Angiogenesis-promoted bone repair with silicate-shelled hydrogel fiber scaffolds

Khandmaa Dashnyam[a,b,#], Jennifer O Buitrago[a,b,#], Tsendmaa Bold[a,b,#], Nandin Mandakhbayar[a,b], Roman A Perez [a,b,c], Jonathan C Knowles[d,e,f,g], Jung-Hwan Lee[a,b,d,g,*], Hae-Won Kim [a,b,d,g,*]

[a]Institute of Tissue Regeneration Engineering (ITREN), Dankook University, Chungcheongnam-do Cheonan 31116, Republic of Korea

[b]Department of Nanobiomedical Science & BK21 PLUS Global Research Center for Regenerative Medicine, Dankook University, Chungcheongnam-do Cheonan 31116, Republic of Korea

[c]UIC Regenerative Medicine Research Institute, Universitat Internacional de Catalunya, Barcelona, Spain

[d]UCL Eastman-Korea Dental Medicine Innovation Centre, Dankook University, Chungcheongnam-do Cheonan 31116, Republic of Korea

[e]Division of Biomaterials and Tissue Engineering, Eastman Dental Institute, University College London, London, UK

[f]The Discoveries Centre for Regenerative and Precision Medicine, Eastman Dental Institute, University College London, London, UK

[g]Department of Biomaterials Science, College of Dentistry, Dankook University, Chungcheongnam-do Cheonan 31116, Republic of Korea

# KD (khandmaa@naver.com), JOB (jenaifer@hotmail.com), and TB (bumbag10@yahoo.com) contributed equally to this work.

Nandin Mandakhbayar (m.nandia@gmail.com), Roman A Perez (rperezan@uic.es), Jonathan C Knowles (j.knowles@ucl.ac.uk)

* Co-corresponding authors: JHL (ducious@gmail.com), HWK (kimhw@dku.edu)

Jung-Hwan Lee, DDS, PhD, Professor, Institute of Tissue Regeneration Engineering (ITREN), Dankook University, Chungcheongnam-do Cheonan 31116, Republic of Korea,

Tel: +82 41 550 3081; Fax: +82 41 559 7839; E-mail: ducious@gmail.

Hae-Won Kim, PhD, Professor, Institute of Tissue Regeneration Engineering (ITREN), Dankook University, Chungcheongnam-do Cheonan 31116, Republic of Korea, Tel: +82 41 550 3081; Fax: +82 41 559 7839; E-mail: kimhw@dku.edu

Abstract

Promoting angiogenesis is a key strategy for stimulating the repair of damaged tissues, including bone. Among other proangiogenic factors, ions have recently been considered a potent element that can be incorporated into biomaterials and then released at therapeutic doses. Silicate-based biomaterials have been reported to induce neovascularization through vascular endothelial growth factor signaling pathway, potentiating acceleration of bone regeneration. Here, we designed a silicate-shelled hydrogel fiber scaffold with a hard/soft layered structure to investigate the possibility of silicate coating on biopolymer for enhancing biological properties. An alginate hydrogel was injected to form a fiber scaffold with shape-tunability that was then coated with a thin silicate layer with various sol-gel compositions. The silicate/alginate scaffold could release calcium and silicate ions, and in particular, silicate ion release was highly sustainable for over one week at therapeutically relevant levels. The ionic release was highly effective in stimulating the mRNA expression of angiogenic markers (VEGF, KDR, eNOS, bFGF, and HIF1-α) in endothelial cells (HUVECs). Moreover, the in vitro tubular networking of cells was significantly enhanced (1.5 times). In vivo implantation in subcutaneous tissue revealed more pronounced blood vessel formation around the silicate-shelled scaffolds than around silicate-free scaffolds. The presence of a silicate shell was also shown to accelerate acellular mineral (hydroxyapatite) formation. The cellular osteogenesis potential of the silicate/alginate scaffold was further proven by the enhanced expression of osteogenic genes (Col1a1, ALP and OCN). When implanted in a rat calvarium defect, the silicate-shelled scaffold demonstrated significantly improved bone formation (2-3 times higher in bone volume and density) with a concurrent sign of proangiogenesis. This work highlights that the surface-layering of silicate composition is an effective approach for improving the bone regeneration

capacity of polymeric hydrogel scaffolds by stimulating ion-induced angiogenesis and providing bone bioactivity to the surface.

Keywords: Angiogenesis, silicate layer, hydrogel scaffold, bone bioactivity, bone repair

Statement of Significance

Among efforts to stimulate the bone repair process, we designed a silicate coated scaffold that can boost angiogenic functions. We take advantage of the roles of ions, particularly silicate ions, by including ions in the composition of the outer part of a polymer hydrogel scaffold. Along with the promotion of angiogenesis, the core-shell design has merits of both a silicate shell and an alginate hydrogel core, i.e., processability, shape formability, sustainable release of ions within a therapeutic range, and bone bioactivity (mineralization) at the surface. The designed scaffold upregulated endothelial cell functions, including the expression of angiogenic markers and tubular formation in vitro and blood vessel growth in vivo. In a defective bone model, the scaffold also significantly accelerated hard tissue formation. This work highlights that the surface functions of polymeric scaffolds with a silicate composition are highly effective for promoting ion-induced angiogenesis and bone bioactivity on the surface and, thus, are ultimately useful for the repair and regeneration of hard tissues.

1. Introduction

Angiogenesis is a key cellular morphogenetic process by which new blood vessels sprout from existing vessels, penetrating a 3D extracellular matrix (ECM) and generating new blood vessel growth to satisfy the local metabolic demand [1, 2]. Promoting angiogenesis has been highlighted as a key strategy in regenerative medicine to stimulate the repair of damaged tissues such as bone, cartilage, muscle, nerve, etc. by supplying sufficient nutrients and oxygen [3-7]. Physiologically, angiogenesis is regulated by a complex interplay of biophysical and biochemical cues, including ECM and angiogenic (growth) factors [8, 9]. Thus, biomaterials have been developed to secrete angiogenic factors and to promote blood vessel growth which consequently leads to increased regenerative potential [10-12].

Among the proangiogenic molecules, ions have recently been considered a potent element that can be incorporated into biomaterials and then released at therapeutic doses [13-20]. In particular, silicate ions enhance a myriad of biological functions of endothelial cells such as migration, homing, tubular formation, and angiogenic gene/protein expression via vascular endothelial growth factor (VEGF) signaling [13, 14]. Moreover, silicate ions have the potential to enhance osteogenic differentiation of stem cells via hydroxyapatite-forming bioactivity [21-25].

Thus, in an effort to stimulate the bone repair process, we designed a scaffold that can boost angiogenic functions by silicate ions. Surface silicate coating, which is a simple yet versatile method to introduce silicate ions into biomaterials, was applied on alginate hydrogel as a model biomaterial. Previously, alginate-silica matrices, fabricated by currently addressed two-step silicate coating on alginate or direct incorporation of bioactive silica-based-nanoparticles, have been investigated with their easy methdology for improved/tunable mechanical and biological properties for a variety of applications, including cell-free or cell-laden regeneratives for (bone) tissue repair, organ on a chip, and biosensing [26-29]. However, the detail investigation of the biological effects of released ions (calcium and silicate) in alginate-silica composite for hard tissue regeneration was not performed, which was nessasary for widespreading application in biomedical field [30, 31].

The design can benefit from the merits of both the silicate shell and the alginate hydrogel core, i.e., processability and shape formability of the core with sustainable release of ions at the therapeutic range and bone bioactivity (mineralization) of the surface, which open the possibility of slicate coating as an widespreading bioactive processe in biomedical field. The pro-angiogenic behaviors of the core-shell scaffold were investigated in terms of the upregulation of endothelial cell functions, including the expression of angiogenic markers and tubular formation in vitro and the blood vessel growth in vivo. Moreover, the acellular mineral (hydroxyapatite) formation and the cellular osteogenesis were tested to examine the bone bioactivity of the scaffold. Lastly, the silicate/alginate scaffold was implanted in a defective bone model to confirm accelerated hard tissue formation with a concurrent sign of pro-angiogenesis. This work is considered to offer a new strategy to develop scaffolds in promoting angiogenesis and bone bioactivity, which ultimately useful for the repair and regeneration of hard tissues.

2. Materials and Methods

2.1 Materials

The reagents for silicate solution were tetraethyl orthosilicate (TEOS) (Sigma-Aldrich, USA, 86578) and 1 N hydrochloric acid standard solution (Daejung, South Korea, 37314). Calcium chloride ($CaCl_2$) (Sigma-Aldrich, US, 383147) and sodium alginate (Duksan, South Korea, d918) were used for the production of alginate-silica fibers.

2.2 Preparation of fiber scaffolds

Sodium alginate (3 % w/v) was prepared in distilled water and placed in a water bath at 37 ºC until homogeneously dissolved. Two different concentrations of silica solution were prepared by mixing TEOS with deionized water (DW) at concentrations of 50% and 80% w/v. Then, 2.4 ml of 0.1 M HCl was added to the mixture as a catalyzer and stirred vigorously for 2-3 h at 400 rpm. A 5 ml syringe loaded with sodium alginate aqueous solution was injected at a ratio of 60 ml/h via an injection pump into an aqueous solution of 300 mM $CaCl_2$ solution through a 17G spinneret needle, and the resulting fiber was kept in the solution for 5 min to allow the alginate polymer to crosslink in the presence of calcium ions. After washing in DW for 2 min, the resulting fibers were immediately immersed in different TEOS solutions (50% and 80%) for 5 min and then dipped in DW 4 times to remove the excess solution prior to any other experimental procedure.

2.3 Hydrogel fiber scaffold characterization

Crosslinked fibers were washed in DW to remove excess calcium ions and/or silica and wiped carefully with ultra-absorbent paper prior to immersion in liquid nitrogen for 5 min. After the ultra-rapid freezing process, scaffolds were cross-sectioned with a blade and lyophilized. Fiber scaffolds were then sputtered with platinum, and the general morphology of the microstructure was observed by a scanning electron microscope (SEM, JEOL-SEM 3000, Hitachi, Japan) equipped with an energy-dispersive X-ray spectrometer to analyze the element composition (EDS, Oxford Instruments, UK). The chemical bond structure of the lyophilized hydrogels was characterized by Fourier transform infrared spectroscopy (Varian 640-IR, Australia). The hydrogel diameter in aqueous solution from different fiber fabrication conditions was optically measured by a microscope (IX71; Olympus, Japan) equipped with metamorph software (n=3).

2.4 Calcium and silicate ion release analysis

The release of silicon and calcium ions from the fiber scaffold was detected by using inductively coupled plasma atomic emission spectrometry (ICP-AES; PerkinElmer, OPTIMA 4300DV). Briefly, each group of fibers (0.3 ml) was immersed and stored in 0.1 M Tris buffer at pH 7 (Sigma-Aldrich, USA, 252859) at 37 ºC. The supernatants were collected for each particular period (12 hours, 1, 3 and 7 days, n=3) and then filtered through a sterile syringe filter for subsequent characterization.

2.5 In vitro pro-angiogenic potential of scaffold

Human umbilical vein endothelial cells (HUVECs) as primary cell obtained from ATCC company (ATCC, US, PCS-100-010) were used in this study to analyze angiogenesis. HUVECs were cultured in vascular cell basal medium (ATCC, US, PCS-100-030) supplemented with an endothelial cell growth kit-VEGF (ATCC, US, PCS-100-041). All animal procedures were performed in accordance with the Guidelines for Care and use of Laboratory Animals of Dankook University and approved by the Animal ethics committee (No.17-011, Dankook University). Cells were incubated in a humidified atmosphere with 5% CO_2 in air at 37 ºC until confluence. Cell behavior was determined by an indirect culture method to analyze the effect of silicon and calcium ions released from fiber scaffolds. First, 3 $\times 10^4$ HUVECs were transferred to each well of 24-well plates and incubated overnight. Then, 0.3 ml fiber scaffolds (culture plates without scaffolds were used as controls) were placed on transwell permeable inserts (Corning; US 353097) on top of seeded cells with 0.5 mL of medium. A Cell Counting Kit-8 (Dojindo Molecular Technologies, Japan, CCK-8) was used to measure cell proliferation for 1, 3 and 7 days (n=5). In brief, for each well, culture growth media was replaced with 200 μL of medium containing 20 μL of CCK-8 solution (10:1) and incubated for 2 h. After incubation, 100 μL of the solution was transferred to a 96-well plate for each well, and optical density was detected by a microplate absorbance reader (iMark; BIO-RAD, US) at 450 nm.

Quantitative analysis of gene expression associated with angiogenesis was confirmed by quantitative real-time PCR (qPCR). A total of $1×10^5$ HUVECs were cultured on each 24-well plate. Similar to a previous experiment, a transwell insert containing a 0.3 ml fiber scaffold was applied to each well of a plate with endothelial growth media. After 24 h of exposure, the total RNA was isolated from harvested cells according to the manufacturer's instructions (GeneAll, South Korea, 304-150). Reverse transcription of 2 μg mRNA was carried out in a thermal cycler (HID Veriti® 96-well Thermal Cycler, Applied Biosystems, US, 4479071) with AccuPower RT-PCR Premix (Bioneer, South Korea, 15030111C) in a mixture of random hexamers and RNAse free water following the manufacturer's instructions. Gene expression was determined by real-time PCR performed in a thermal cycler (StepOne™ Plus, Applied Biosystems, US) with RealAmp™ SYBR qPCR Master mix (GeneAll Biotechnology, South Korea, 801-051). The relative gene expression levels were calculated using the comparative Ct method ($2^{-ΔΔCt}$) and normalized with respect to endogenous human GAPDH gene expression. The primers used for angiogenesis gene amplification are shown in Table 1 (n=3).

Tubular network formation was examined by culturing HUVECs on a

Matrigel™ matrix (BD Biosciences, US, 356234). A 24-well plate surface was covered with Matrigel™ for 15 min at 37 ºC as specified by the manufacturer`s guidelines. Following gelation, 1×10^3 cells were seeded onto Matrigel homogenously, and then, 0.3 ml fiber scaffolds were loaded onto the transwell inserts and placed in each well. Tubular morphology was observed using an inverted light microscope (IX71; Olympus, Japan) at different time points (n=5, 0, 7, and 12 h). For each group, triplicate samples were performed, and random fields were photographed to analyze the angiogenesis assay. Total tubule length, the numbers of nodes (branch points), and circles (mesh-like circles) were analyzed by using ImageJ software.

2.6 In vivo angiogenesis in the subcutaneous model

In vivo biocompatibility and neo-vessel formation ability were evaluated by implanting the fiber scaffolds under the subcutaneous tissue of 6-week-old Sprague-Dawley male rats and analyzing at different time points (2 and 4 weeks, n=4). Four replicates for each experimental group (Si0%, Si50%, and Si80%) were used for this study. The animals were cared for in individual cages under a controlled environment with food and water provided *ad libitum* following guidelines accepted by the Animal Care and Use Committee of Dankook University, Cheonan Campus, South Korea (DKU 17-011).

The animal surgery was performed under anesthetic conditions by intramuscular injection of ketamine/xylazine. The dorsal area of the skin was shaved and sterilized with 70% ethanol and povidone solution. Fiber scaffolds (0.5 mL) from different experimental groups were implanted in separate pockets made under the skin on both lateral sides of the spine. Furthermore, the incision was closed by non-absorbable suture material (4-0 Prolene, Ethicon, Germany), and animals were sacrificed prior to histological analysis at each time point. The implanted scaffold area was extracted and fixated with 10 % neutral buffered formalin for 24 h at room temperature. The specimens were dehydrated in an ordered gradient of ethanol, bisected and embedded in paraffin. Histological sections of 5 μm were cut by a microtome (Leica RM2245, Leica™, Biosystems, Germany). Finally, samples were stained by hematoxylin and eosin (H&E) using a routine procedure and analyzed under an optical light microscope (IX71, Olympus, Japan).

2.7 In vitro acellular bone bioactivity

The apatite-forming ability of fiber scaffolds was estimated by incubating 0.5 ml of samples from each group placed in a 15-ml tube with 10 ml of simulated body fluid (2x SBF) at 37 ºC for 14 days. To check hydroxyapatite formation, hydrogels were washed carefully in distilled water, freeze-dried overnight, and examined by SEM and X-ray diffraction (Rigaku, Ultima IV, Japan).

2.8 Osteogenic potential of scaffold

The isolation of rat mesenchymal cells was performed following a previous protocol published by our group elsewhere[32]. Cells were cultured on TCP substrate at a ratio of 6250 cells/cm^2 and incubated for 24 h prior to any experiment. At the same time, alginate and silicate-alginate fibers were immersed in alpha-modified MEM (Welgene, South Korea, LM 008-53) and incubated for 24 h at 37 ºC. The next day, both conditioned media were collected, filtered and supplemented with 10% fetal bovine serum (FBS) (Corning, USA, 35-015-CV), 1% penicillin-streptomycin (Gibco, USA, 15140-122), and osteogenic factors (10 mM β-glycerol phosphate, 10 nM dexamethasone and 50 μg/mL ascorbic acid). Cells were exposed to different osteogenic conditioned media and compared with the control group for further characterization at several time points (7-28 day). The media were refreshed every other day. The osteogenic differentiation of rat MSCs was analyzed by qPCR following the above-mentioned protocol, and the primers used are listed in Table 1 (n=3).

2.9 In vivo bone formation study

For this animal study, healthy male Sprague-Dawley rats (9 - 10-week-old) were used. The animal care and experimental protocols were approved by the Animal Care and Use Committee of Dankook University, Cheonan Campus, South Korea (DKU 17-011). Animals were housed in cages under constant temperature in a humidity-controlled environment, exposed to a 12 h light-dark cycle and had free access to water and food. Two study groups (n=5; Si0% and Si80%) were selected for our *in vivo* study. Animals were randomly selected for implantation of 1.5 mL fiber scaffolds in each rat calvaria defect under general anesthesia by an intramuscular injection of the mixture (ketamine 80 mg/kg and xylazine 10 mg/kg).

After shaving over the cranial lesion, the surgical site was wiped with iodine and 70% ethanol, and a linear skin incision was made by a surgical blade (No. 10). A full-thickness flap was peeled away, and the calvarial bone was exposed. In each rat, a 5 mm diameter calvarial bone defect was made on the right and left sides of the parietal bone under cooling conditions with sterile saline using a dental hand-piece and a 5 mm diameter trephine drill (GHI, Pakistan). The subcutaneous tissues and periosteum were sutured with absorbable sutures (4-0 Vicryl®, Ethicon, Germany), and the skin was folded with non-absorbable suture material (4-0 Prolene, Ethicon, Germany).

Afterward implantation of the samples, the animals were supervised regularly for possible clinical signs of infection, inflammation, and any injurious reaction. At six weeks postoperation, the animals were euthanized by CO_2 inhalation, and the tissue surrounding the calvarium defect with the implantation was harvested and fixed in 10% neutral buffered formalin for 24 h at room temperature. The harvested samples were kept for histological and micro-CT analysis.

2.10 Analyses by micro-CT and histology

After sample fixation, micro-computed tomography (μ-CT) imaging was performed (Skyscan 1176, Skyscan, Aartselaar, Belgium) with X-ray at 65 kV and 385 μA, with an exposure time of 279 ms for each section (μm). Images reconstructed from the scanned images were used to analyze hard tissue formation over the region of interest using CTAn Skyscan software; new hard tissue volume (mm^3), new bone volume (mm^3), and bone surface density (BS/BV) (1/mm) in the defect area. 3D images were formulated and visualized by CTvol Skyscan software (ver. 2.3.2.0).

For the histological analysis, fixed tissues were decalcified in RapidCal™ solution (BBC Chemical Co., USA) for five days. After decalcification, the samples were dehydrated in a series of ethanol solutions of increasing concentration and then embedded in paraffin. Using a semi-automated rotary microtome (Leica RM2245, Leica Biosystems, Germany), five-micrometer coronal sections of the central area of the samples were prepared and then transferred to coated glass slides. The slides with tissue sections were deparaffinized and hydrated through a series of xylene and graded ethanol solutions and were finally stained with H&E for the estimation of new bone area. Histological sections were visualized under a light microscope (IX71, Olympus, Japan).

2.11 Statistical analysis

Experiment assays were performed in triplicate unless otherwise specified, and data were expressed as the mean ± one standard deviation. Statistical analysis was performed by T-student for μ-CT data and one-way analysis of variance (ANOVA) with the Bonferroni post hoc correction for the rest of the assays. Significance was considered at $p < 0.05$ unless otherwise stated.

3. Results and discussion

3.1 Preparation of scaffolds and the properties

Biomaterials have been developed to increase angiogenesis by delivery of biomolecules and drugs to the target site for the regeneration of tissues including bone [3, 21, 22, 33]. Among other proangiogenic factors, ions have recently been highlighted as potent elements that can be incorporated into biomaterials. Here, we focused on the role of silicate ions as the pro-angiogenic element for bone regeneration [34-36]. Thus, the scaffold was designed to be a core-shell structure that has the merits of both shape-formability of alginate hydrogel and pro-angiogenic and bone-bioactive capacity of silicate [35-38]. Even though alginate-silica matrices have been investigated with their easy methodology for improved/tunable mechanical or biological properties for a variety of applications, including cell-free or cell-laden regeneratives for (bone) tissue repair, organ on a chip, and biosensing[26-29], the detail investigation of indirect effect from alginate-silica core-shell composite was not performed yet, especially with the focus on the released ions (calcium and silicate) and their therapeutic efficacy[30, 31].

Alginate hydrogel fiber scaffolds were successfully fabricated by the injection of sodium alginate solution using a spinneret needle with the help of a pumping system under a constant flow rate and crosslinked in a calcium chloride bath (Fig. 1a). The rapid crosslinking of alginate occurred in the presence of calcium ions and allowed fiber architectures to be maintained, as previously reported [39]. First, 3% w/v alginate solution concentration was chosen due to its stability for holding the fiber shape [35] whereas 1% w/v alginate fiber was brittle and 5% w/v alginate fiber formed beads due to high viscosity. The size of alginate hydrogels was then optimized by varying processing conditions: solution injection speed (20 and 60 ml/h), calcium concentration (150, 300 and 500 mM) and crosslinking time (5 and 60 min), as presented **in Supp. 1**. The condition of flow rate 60 ml/h, 300 mM $CaCl_2$, and incubation time 5 min was chosen for further studies.

With the fiber scaffolds, sol-gel silicate was then dip-coated while the concentration of silicate was varied (Fig. 1b). As represented in Fig. 1c, even though silicate shell conferred some rigidity to the alginate fiber scaffold, both shelled (Si80%) and unshelled (Si0%) fiber scaffolds were easily molded and implantable to any particular shape. The morphology of alginate fibers with or without silicate shell, as observed by SEM (Fig. 2a), revealed different surface textures (wavy in Si0% versus dry lava-like in Si80%). EDS with mapping confirmed a thin outer layer in Si80% to be Si-rich (white arrow, **Supp. 2**). FT-IR spectra showed typical silicate-related bands (Si-O-Si at 413 and 418 cm^{-1}, Si-O peak at 556 cm^{-1}, Si-H stretching at 943 and 927 cm^{-1} and C-H stretching at 2891 and 2874 cm^{-1}) in the silicate-shelled scaffolds while alginate-related peaks (C-O-H stretching at 1403 cm^{-1}, C-O stretching at 1585 and 1619 cm^{-1}, and O-H stretching at 1010 cm^{-1} and 3000 ~ 3500 cm^{-1}) were observed in all groups (Fig.

2b).

Next, the ionic release behavior of the fibers was examined in Tris buffer up to 7 days by ICP-AES (Fig. 2c). In the first 12 hr of the immersion, the amount of silicate ion released from Si80% was ~85 ppm, and the amount doubled to ~160 ppm by 24 hr. The more sustained release was observed at longer incubation times, reaching a final amount of 326 ppm by the end of the experiment at 7 days. The Si0% group showed no release of silicate ions, while calcium ions were more highly released from the Si0% group than the Si80% group. The calcium release is due to the hydrolysis of weak interactions between calcium and alginate monomers [32], and the silicate shell might reduce the calcium release from the inner alginate hydrogel. The results on ionic releases (silicate ions of ~47 ppm/day and calcium ions of 11~23 ppm/day) suggest the possible role of ions from the silicate/alginate scaffold in influencing the cellular responses such as angiogenesis and osteogenesis [13-15, 21, 22]. Along with succeful fabrication of other biopolymer-silica composite, it was assumed that above silicate coating could induce additional therapeuric ion (silicate) with minimal mitigation of core biomolecules/ions, and consequently accelearte biological efficacy[30, 31, 40].

Particularly for bone regeneration, the large amount of silicate ions released initially from the outer surface is beneficial for an early-angiogenic induction process, and the more slowly released calcium ions from the inner part might also support further osteogenic process.

3.2 *In vitro* stimulation of endothelial cells

The angiogenic effects on HUVECs, a model human endothelial cell type, with scaffold were assessed by the indirect method to investigate angiogenic gene expression and tubular formation from the released ions in biomaterials. First, a cell toxicity assay was performed indirectly with transwell inserts (Fig. 3a). The results demonstrate that cell viability is similarly increased with time up to 3 days in the fiber groups, suggesting that no toxicity from fibers developed. Then, the effects of fiber scaffolds on the angiogenic gene expression of HUVECs were measured by qPCR (Fig. 3b-f). The expression of angiogenesis-related genes, such as VEGF, HIF-1α, KDR, bFGF and eNOS, was analyzed at 24 h. The gene expression levels of VEGF and its receptor KDR were significantly upregulated up to 2~2.5-fold in silica-shelled groups (Si50% or Si80%) compared with the control cell group ($P<0.05$). In particular, the expression of other angiogenic genes, such as eNOS, bFGF and HIF1-α, was significantly higher in silica-shelled fibers (Si50% or Si80%) by up to 4~20-fold compared with pristine fibers (Si0%, $P<0.05$ or $P<0.001$). The results demonstrate that the silicate ion released from the fiber scaffolds, especially Si80%, has a significant effect on stimulating angiogenic gene expressions.

Next, an *in vitro* tubular formation assay was performed. HUVECs were cultured on Matrigel, and the insert, including the fiber hydrogel, was placed on top of the Matrigel, thus allowing ionic interactions of cells. Optical morphologies (at 0, 7, 12 hr) and live calcein stained cells (at 12 hr) were visualized to investigate the tubular forming ability and live status of cells, respectively (Fig. 4a). The tubular networking, such as the number of tubular circles, the number of nodes, and the total tubule length, were then quantified (Fig. 4b). At an earlier period (7 hr), Si80% demonstrated a significant increase by ~50% in the number of tubular circles and nodes compared with the cell-only control or Si0% ($P<0.05$) and displayed improved neovascularization in Si80% compared with Si0%. The decreasing number of circles and nodes at 12 hr compared with 7 hr may be due to the process of tubular formation followed by an increase in tubular length [14, 41].

3.3 *In vivo* blood vessel formation

To analyze the *in vivo* neo-blood vessel formation, scaffolds were subcutaneously implanted in 6-week-old rats for 4 weeks. H&E staining images were taken up at 2 and 4 weeks, as shown in Fig. 5. Results presented no severe tissue toxicity and inflammation around the implanted materials. Neo-blood vessels with red blood cells were stained in dark red, as indicated by red arrows, revealing more blood vessels formed in Si80% than in Si0%. Based on images, the total number and area of blood vessels and the diameter distribution were quantitively measured, and the results revealed a significant increase in the total number and area of blood vessels in the silica-shelled groups (Si50% or Si80%)

by up to 3~10 times compared with Si0% group ($P<0.05$). The distribution of the diameter of blood vessels revealed a greater fraction of large diameter blood vessels in Si80% than in Si0% and Si50%, and there was significant difference in Si80% compared to others ($P<0.05$). Taken together, silicate ions released from silica-shelled fiber hydrogels (especially Si80%) are considered to get heavily involved in stimulating neo-blood vessel formation *in vivo* while preserving excellent biocompatibility without severe inflammation.

3.4 Acellular apatite-forming ability and cellular osteogenesis

Along with the angiogenic capacity, the osteogenic property is of high importance for use as bone regenerative materials. First, we observed the acellular bone bioactivity by means of apatite forming ability of the scaffolds in SBF (Fig. 6a and b). The SEM image of Si80% fiber scaffolds after immersion in SBF showed typical apatite crystal growth on the surface, while the mineralization process did not progress under the same conditions in Si0%. This phenomenon can be explained similarly to the bioactive silicate-based materials [21, 22], i.e., the sequential processes of calcium ions release, the precipitation of calcium and phosphate ions on the hydrated silicate layer enriched with silanol groups, and the consequent formation of calcium phosphate crystals with time [42, 43]. The XRD spectra revealed apatite-related diffraction peaks at 2θ~27°, ~32° and ~46° after the immersion in SBF, with higher apatite peak intensities noted in Si80%, confirming the silica-shelled scaffolds improved bone-like mineral formation ability [43].

Next, we tested the cellular osteogenic stimulation of the Si80% scaffolds versus Si0% based on the angiogenic analysis, revealing the most prominent angiogenic potential in Si80% among groups and, consequently, more potential to encourage osteogenesis[44, 45]. Conditioned medium collected after immersing the Si0% and Si80% scaffolds for 24 hr were treated to rMSCs. After cultures for 2 weeks, the osteogenic gene expression was analyzed by qPCR (Fig. 6c). Compared with the control (OM), Si0% had no effect on increasing osteogenic gene expression, while Si80% was able to significantly increase the osteogenic gene expression, including not only early markers, such as collagen type I and alkaline phosphatase but also a late marker, osteocalcin, by up to 1.5~4-fold. In particular, Si80% revealed a significant increase in the expression of all osteogenic genes by up to 1.8~4-fold compared with Si0%, demonstrating that the significant role of released ions in stimulating osteogenesis of stem cells [46]. In this work, the effect of calcium ions was not well revealed as there was no significant increase by the extracts from Si0%, although calcium ions are known to be involved in osteogenic differentiation via calcium-signaling activation [47-50]; rather, the combined role of silicate ions with calcium ions through Si80% appeared to be more explicit in the osteogenic stimulation of rMSCs along with previous literatures[51, 52], and the exact mechanism underlying this in vitro cellular event remains further in-depth study.

3.5 Early bone formation

Finally, the potential of early bone formation of the scaffolds was investigated in the round-shaped defect model in rat calvaria for six weeks. The fibrous morphology of the hydrogel-based scaffolds allowed easy handling and shaping into the created bone defect. In harvested tissue, no severe inflammation was observed near the implantation area at the time of sacrifice. The μ-CT 3D images showed more new bone formation in Si80% than in Si0% within the defect regions, as indicated by the red-brown area (new bone) (Fig. 7a**).** According to the quantitative data regarding bone quantity and quality (bone volume (BV), surface area (BS), tissue volume (TV) and bone surface density (BSD), in Fig. 7c), the Si80% group clearly exhibited up to 3 times more bone formation than the Si0% group ($P<0.05$ or $P<0.01$).

The samples were further histologically analyzed after H&E and Masson's trichrome (MT) staining. Both H&E and MT stained images demonstrated more new bone matrix formed within the healing area in Si80% (Fig. 7b**)**. Of note, the Si80% presented more blood vessels ('*') than Si0%, highlighting the promoted angiogenesis in the silicate-shelled scaffold. Also, the collagen content was higher in Si80% than in Si0%, indicating the higher collagen deposition might help to improve the bone healing and maturation process. The *in vivo* results demonstrated that the silicate-shelled scaffolds significantly enhanced early bone formation with a concurrent stimulation of angiogenic events.

4. Conclusion

We designed a scaffold that can boost angiogenic functions by silicate ions which leads to stimulated bone repair process by accelerated angiogenesis. Surface silicate coating, which is a simple yet versatile method to introduce silicate ions into biomaterials, was applied on alginate hydrogel as a model biomaterial to modify the composition of the outer part of a polymer hydrogel scaffold. Along with the promotion of angiogenesis, the core-shell design has merits of both a silicate shell and an alginate hydrogel core, i.e., processability, shape formability, sustainable release of ions within a therapeutic range, and bone bioactivity (mineralization) at the surface. The loaded ions could be sustainably released within the therapeutic range for over one week, inducing angiogenesis and bioactivity (mineralization) at the surface for osteogenesis. The designed scaffold upregulated endothelial cell functions, including the expression of angiogenic markers (~20 times) and tubular formation in vitro (~50% more) and blood vessel growth in vivo (~10 times). In a defective bone model, the scaffold also significantly accelerated hard tissue formation (~3 times). This work highlights that the surface functions of polymeric scaffolds with a silicate composition are highly effective for promoting ion-induced angiogenesis and bone bioactivity on the surface and, thus, are ultimately useful for the repair and regeneration of hard tissues.

Acknowledgment

This work was supported by the National Research Foundation of Korea (NRF) via a grant funded by the Ministry of Science and ICT (NRF-2019R1C1C1002490, 2018R1A2B3003446 and 2018K1A4A3A01064257 (Global Research Development Center Program) and the Ministry of Education (2019R1A6A1A11034536).

Statement

The researcher claims no conflicts of interest

References

1. P. Carmeliet, *Nature*, 2005, **438**, 932-936.
2. M. Potente, H. Gerhardt and P. Carmeliet, *Cell*, 2011, **146**, 873-887.
3. H. S. Kim, X. Sun, J.-H. Lee, H.-W. Kim, X. Fu and K. W. Leong, *Adv. Drug Deliv. Rev.*, 2018.
4. A. Torres, S. Bidarra, M. Pinto, P. Aguiar, E. Silva and C. Barrias, *Biomaterials*, 2018, **154**, 34-47.
5. C. E. Nelson, A. J. Kim, E. J. Adolph, M. K. Gupta, F. Yu, K. M. Hocking, J. M. Davidson, S. A. Guelcher and C. L. Duvall, *Adv. Mater.*, 2014, **26**, 607-614.
6. R. Jin, G. Song, J. Chai, X. Gou, G. Yuan and Z. Chen, *J. Tissue Eng.*, 2018, **9**, 2041731418817505.
7. J. B. Norelli, D. P. Plaza, D. N. Stal, A. M. Varghese, H. Liang and D. A. Grande, *J. Tissue Eng.*, 2018, **9**, 2041731418811183.
8. M. M. Martino, P. S. Briquez, K. Maruyama and J. A. Hubbell, *Adv. Drug Deliv. Rev.*, 2015, **94**, 41-52.
9. P. Carmeliet, *Nat. Med.*, 2003, **9**, 653.
10. N. Mitrousis, A. Fokina and M. S. Shoichet, *Nat. Rev. Mater.*, 2018, **3**, 441-456.
11. P. S. Briquez, L. E. Clegg, M. M. Martino, F. M. Gabhann and J. A. Hubbell, *Nat. Rev. Mater.*, 2016, **1**, 15006.
12. A. Thakur, S. Mishra, J. Pena, J. Zhou, S. Redenti, R. Majeska and M. Vazquez, *J. Tissue Eng.*, 2018, **9**, 2041731417751286.

13. K. Dashnyam, G.-Z. Jin, J.-H. Kim, R. Perez, J.-H. Jang and H.-W. Kim, *Biomaterials*, 2017, **116**, 145-157.

14. K. Boldbaatar, K. Dashnyam, J. C. Knowles, H.-H. Lee, J.-H. Lee and H.-W. Kim, *Acta Biomater.*, 2019, **83**, 322-333.

15. K. Dashnyam, A. El-Fiqi, J. O. Buitrago, R. A. Perez, J. C. Knowles and H.-W. Kim, *J. Tissue Eng.*, 2017, **8**, 2041731417707339.

16. Y. Brudno, A. B. Ennett-Shepard, R. R. Chen, M. Aizenberg and D. J. Mooney, *Biomaterials*, 2013, **34**, 9201-9209.

17. M. M. Martino, S. Brkic, E. Bovo, M. Burger, D. J. Schaefer, T. Wolff, L. Gürke, P. S. Briquez, H. M. Larsson and R. Gianni-Barrera, *Front. Bioeng. Biotechnol.*, 2015, **3**, 45.

18. V. A. Kumar, N. L. Taylor, S. Shi, B. K. Wang, A. A. Jalan, M. K. Kang, N. C. Wickremasinghe and J. D. Hartgerink, *ACS Nano*, 2015, **9**, 860-868.

19. J.-H. Kim, T.-H. Kim, M. S. Kang and H.-W. Kim, *Biomed. Res. Int.*, 2016, **2016**, 8.

20. G. Fernandez de Grado, L. Keller, Y. Idoux-Gillet, Q. Wagner, A.-M. Musset, N. Benkirane-Jessel, F. Bornert and D. Offner, *J. Tissue Eng.*, 2018, **9**, 2041731418776819.

21. J.-H. Lee, A. El-Fiqi, N. Mandakhbayar, H.-H. Lee and H.-W. Kim, *Biomaterials*, 2017, **142**, 62-76.

22. J.-H. Lee, N. Mandakhbayar, A. El-Fiqi and H.-W. Kim, *Acta Biomater.*, 2017, **60**,

93-108.

23. P. Han, C. Wu and Y. Xiao, *Biomater. Sci.*, 2013, **1**, 379-392.

24. A. El-Fiqi, J.-H. Kim, R. A. Perez and H.-W. Kim, *J. Mater. Chem. B Mater. Biol. Med.*, 2015, **3**, 1321-1334.

25. J.-J. Kim, A. El-Fiqi and H.-W. Kim, *ACS Applied Materials & Interfaces*, 2017, **9**, 2059-2073.

26. U. Schloßmacher, H. C. Schröder, X. Wang, Q. Feng, B. Diehl-Seifert, S. Neumann, A. Trautwein and W. E. Müller, *RSC Adv.*, 2013, **3**, 11185-11194.

27. J. Venkatesan, I. Bhatnagar, P. Manivasagan, K.-H. Kang and S.-K. Kim, *Int. J. Biol. Macromol.*, 2015, **72**, 269-281.

28. M. Perullini, M. Calcabrini, M. Jobbágy and S. A. Bilmes, *Open Material Sciences*, 2015, **2**, 3-12.

29. A. Pannier, U. Soltmann, B. Soltmann, R. Altenburger and M. Schmitt-Jansen, *J. Mater. Chem. B Mater. Biol. Med.*, 2014, **2**, 7896-7909.

30. H. Lee, Y. Kim, S. Kim and G. Kim, *J. Mater. Chem. B Mater. Biol. Med.*, 2014, **2**, 5785-5798.

31. K. Jahan and M. Tabrizian, *Biomater. Sci.*, 2016, **4**, 25-39.

32. J. Olmos Buitrago, R. A. Perez, A. El-Fiqi, R. K. Singh, J.-H. Kim and H.-W. Kim, *Acta Biomater.*, 2015, **28**, 183-192.

33. K. D. Patel, R. K. Singh and H.-W. Kim, *Mater. Horiz.*, 2019, **6**, 434-469.

34. K. Y. Lee and D. J. Mooney, *Prog. Polym. Sci.*, 2012, **37**, 106-126.

35. P. R. A., K. Meeju, K. Tae-Hyun, K. Joong-Hyun, L. J. Ho, P. Jeong-Hui, K. J. C. and K. Hae-Won, *Tissue Eng. Part A*, 2014, **20**, 103-114.

36. R. A. Perez, J.-H. Kim, J. O. Buitrago, I. B. Wall and H.-W. Kim, *Acta Biomater.*, 2015, **23**, 295-308.

37. J.-H. Lee and H.-W. Kim, *J. Tissue Eng.*, 2018, **9**, 2041731418768285.

38. G.-Z. Jin and H.-W. Kim, *J. Tissue Eng.*, 2018, **9**, 2041731418802438.

39. R. A. Perez and H.-W. Kim, *J. Biomed. Mater. Res. A*, 2013, **101A**, 1103-1112.

40. M. L. Foglia, D. E. Camporotondi, G. S. Alvarez, S. Heinemann, T. Hanke, C. J. Perez, L. E. Diaz and M. F. Desimone, *J. Mater. Chem. B Mater. Biol. Med.*, 2013, **1**, 6283-6290.

41. A. Chervin-Pétinot, M. Courçon, S. Almagro, A. Nicolas, A. Grichine, D. Grunwald, M.-H. Prandini, P. Huber and D. Gulino-Debrac, *J. Biol. Chem.*, 2012, **287**, 7556-7572.

42. A. Hoppe, N. S. Güldal and A. R. Boccaccini, *Biomaterials*, 2011, **32**, 2757-2774.

43. G. R. Beck, S.-W. Ha, C. E. Camalier, M. Yamaguchi, Y. Li, J.-K. Lee and M. N. Weitzmann, *Nanomedicine: Nanotechnology, Biology and Medicine*, 2012, **8**, 793-803.

44. A. Grosso, M. G. Burger, A. Lunger, D. J. Schaefer, A. Banfi and N. Di Maggio, *Front. Bioeng. Biotechnol.*, 2017, **5**, 68.

45. Y. Jia, Y. Zhu, S. Qiu, J. Xu and Y. Chai, *Stem Cell Res. Ther.*, 2019, **10**, 12.

46. A. I. Rodrigues, M. B. Oliveira, J. F. Mano, M. E. Gomes, R. L. Reis and I. B.

Leonor, *ACS Biomater. Sci. Eng.*, 2015, **1**, 760-770.

47. A. M. C. Barradas, H. A. M. Fernandes, N. Groen, Y. C. Chai, J. Schrooten, J. van de Peppel, J. P. T. M. van Leeuwen, C. A. van Blitterswijk and J. de Boer, *Biomaterials*, 2012, **33**, 3205-3215.
48. F. Viti, M. Landini, A. Mezzelani, L. Petecchia, L. Milanesi and S. Scaglione, *PLoS One*, 2016, **11**, e0148173.
49. G.-Y. Jung, Y.-J. Park and J.-S. Han, *Journal of Materials Science: Materials in Medicine*, 2010, **21**, 1649-1654.
50. S.-K. Jun, J.-H. Lee and H.-H. Lee, *Biomed. Res. Int.*, 2017, **2017**, 9.
51. S. Saravanan, S. Vimalraj, M. Vairamani and N. Selvamurugan, *J. Biomed. Nanotechnol.*, 2015, **11**, 1124-1138.
52. W. Zhai, H. Lu, C. Wu, L. Chen, X. Lin, K. Naoki, G. Chen and J. Chang, *Acta Biomater.*, 2013, **9**, 8004-8014.

Table 1. Primer sequences for qPCR

	Gene	Forward (5'-3')	Reverse (5'-3')
Housekeeping gene	Rat GAPDH	CAAGGATACTGAGAGCAAGAG	ATGGAATTGTGAGGGAGATG
	Human GAPDH	GATTTGGTCGTATTGGGCG	CTGGAAGATGGTGATGG
Angiogenic markers	VEGF	TGCGGATCAAAC CTCACCA	CAGGGATTTTT CTTGTCTTGCT
	KDR	GTGATCGGAA ATGACACTGGAG	CATGTTGTTCAC TAACAGAAGCA
	HIF1α	CCATGTGACCA TGAGGAAAT	CGGCTAGTTAGGG TACACTT
	eNOS	TGTCCAACATGC TGCTGGAAATTG	AGGAGGTCTTCTTCCTGGTGATGCC
	bFGF	CAATTCCCATGTGCTGTGAC	ACCTTGACCTCTCAGCCTCA
Osteogenic markers	ALP	CTCTGCCGTTGTTTCTCTAT	AGGTGCTTTGGGAATCTG
	COL1A1	CTGGTACATCAGCCCAAAC	GAACCTTCGCTTCCATACTC
	BSP	GTACATCTGAACGGCTAAGG	GTTTGGTAAATCTGGCAACTC
	OCN	GCTTCAGCTTTGGCTACT	CGTTCCTCATCTGGACTTTAT

Figure Legends

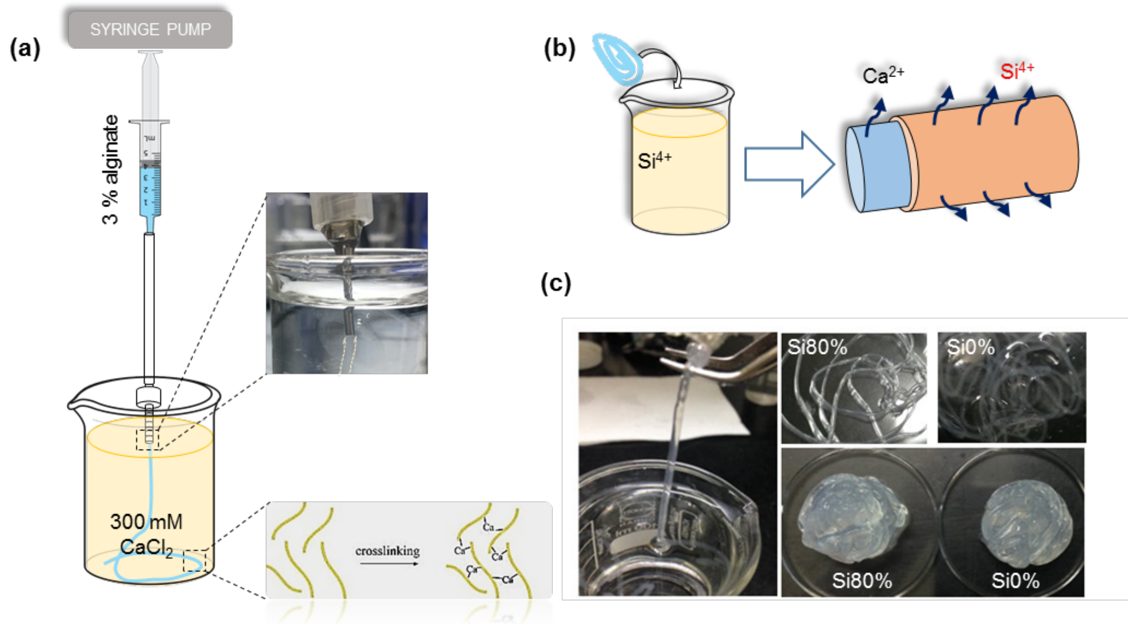

Figure 1. Production of silica-coated alginate hydrogel fiber (a) Schematic showing the equipment setup for fabricating alginate hydrogel fiber scaffolds. Sodium alginate solution was flushed through a spinneret needle at a constant rate of 60 ml/h with a pumping device, which was injected into a 300 mM calcium chloride bath, resulting in a hydrogel fiber due to the physical crosslinking of calcium ions with alginate. (b) Alginate hydrogel fibers were coated with a thin layer of silica by immersing the fibers in a silica solution (50 % or 80 %) for 5 min. Hypothetically, Si^{4+} was released from the external coated layer, while Ca^{2+} was released from the crosslinked alginate scaffold. (c) Optical images of the hydrogel carrier revealed a continuous fiber texture, which can be easily molded into different shapes before and after silicate coating.

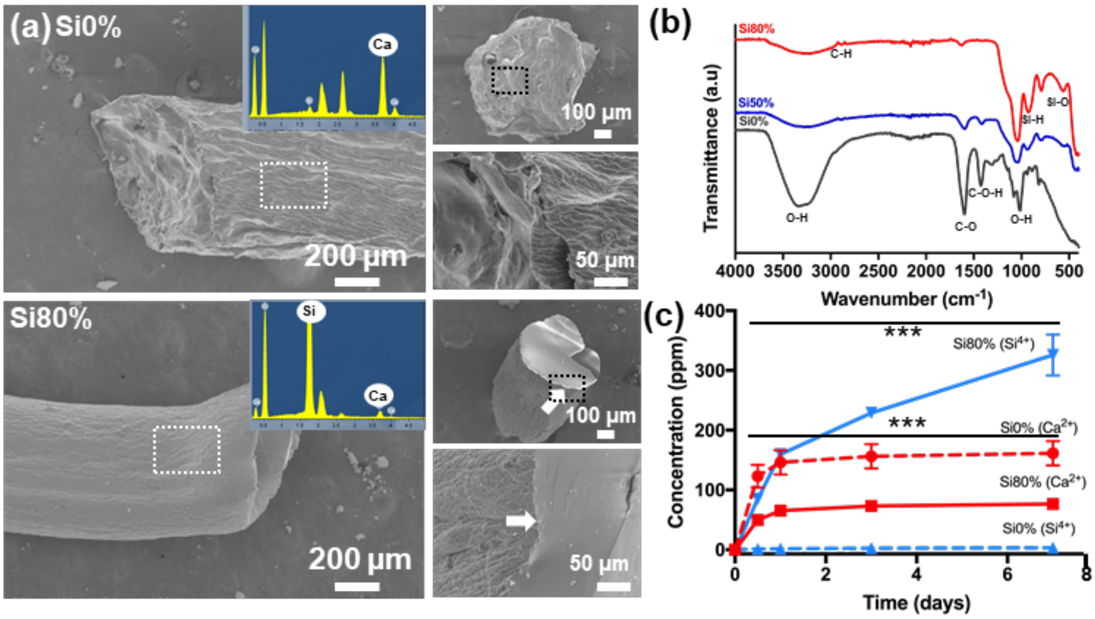

Figure 2. Physico-chemical characterization of silica-coated alginate hydrogel fibers. (a) Representative SEM and EDX results of silicate-free (Si0%) and silicate-shelled (Si80%) alginate fibers, revealing a thin layer of silicate coating (white arrow). (b) FTIR spectrum of fiber scaffolds as given status showing chemical bonds of alginate (Si0%) and silica-shelled alginate scaffolds (Si50%, Si80%). The result showed Si-O bonding in the silicate coating groups (Si50% and Si80%). (c) Si^{4+} and Ca^{2+} ion release test from scaffolds analyzed in Tris-HCl buffer at different time point up to 1 week. Ca^{2+} was released over a week at therapeutically relevant levels from all scaffolds as a result of degradation of the alginate hydrogel fiber, whereas Si^{4+} was released only from the outer silica coating layer from the silica group (significant difference between Si0% and Si80%, *** $p<0.001$, n=3).

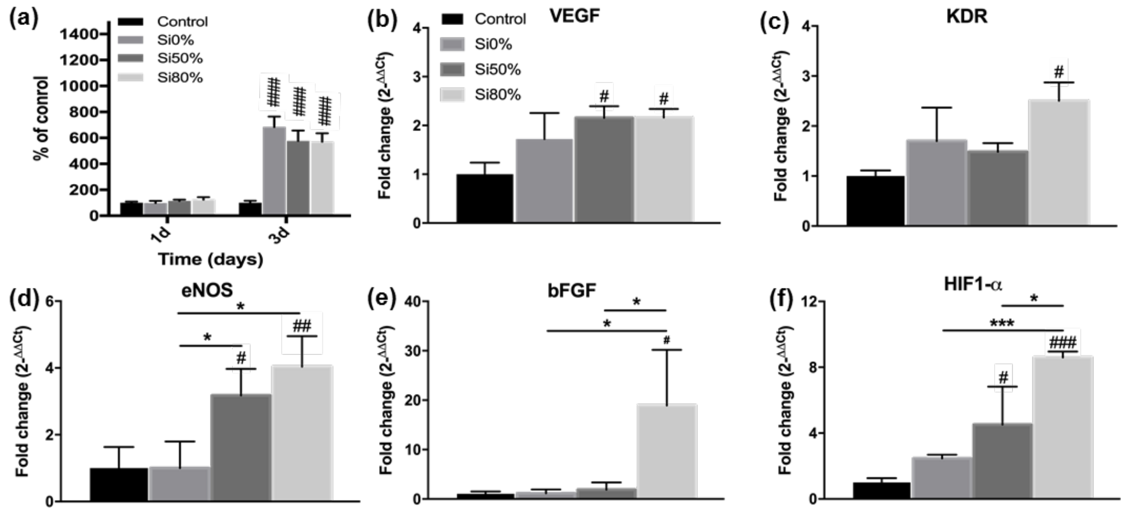

Figure 3. Cytotoxicity and angiogenic gene expression of silica-coated alginate hydrogel fibers cultured indirectly with endothelial cells. (a) The indirect effect of fiber scaffolds on the proliferation of endothelial cells was studied with transwell membranes and HUVECs for up to 3 days. (b-f) The expression of angiogenic-related genes, including VEGF, KDR, eNOS, bFGF and HIF-1α, was assessed by quantitative qPCR. The release of ions from the scaffolds was highly effective in stimulating the mRNA expression of angiogenic markers (VEGF, KDR, eNOS, bFGF, and HIF1-α) in endothelial cells (HUVECs) without negative effects on proliferation. (Statistical difference between groups, # $p<0.05$ and ### $p<0.001$ in comparison with control cells w/o fibers and *$p<0.05$, *** $p<0.001$, **** $p<0.0001$ for comparison between fiber scaffold; n=5 for cell viability, n=3 for qPCR).

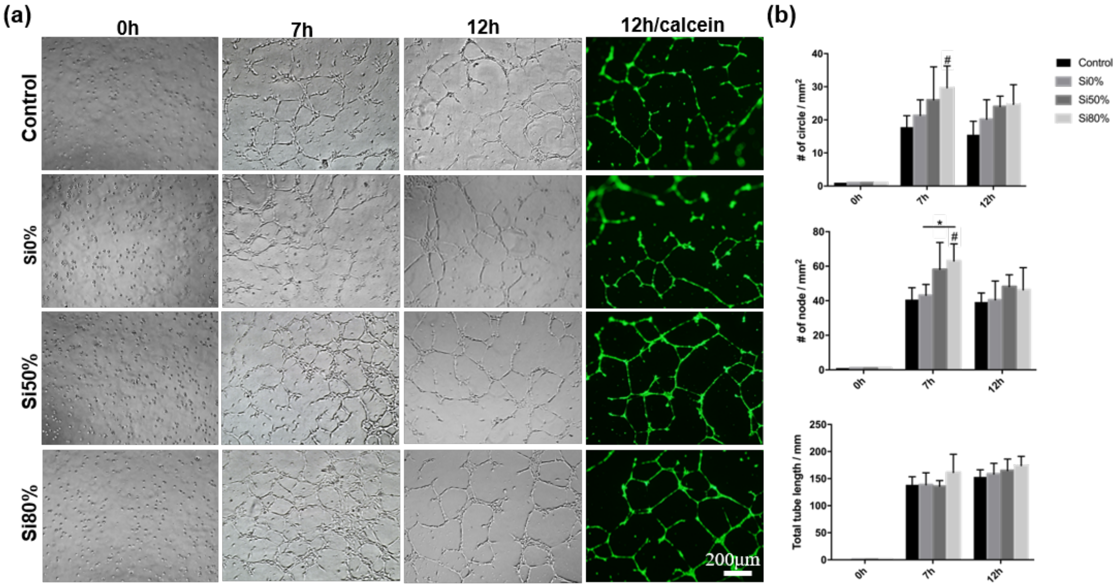

Figure 4. Angiogenic tubular formation of endothelial cells from silica-coated alginate hydrogel fibers. Tubular networking of endothelial (HUVECs) cell responses to the therapeutic ions from the fibrous structured scaffolds (transwell inserts were used). (a) Tubular formation on Matrigel and a calcein-positive green fluorescence image showing stained live cells obtained from each group (control, different silicate concentrations of 0, 50 and 80%) at 0, 7 or 12 hr. Enhanced tubular formation appeared in Si50% and Si80% at 7 hr without dead cells at 12 hr. (b) The number of circles, the number of nodes and the total tube length were quantified. The in vitro tubular networking of cells (especially the number of nodes) was significantly enhanced (1.5 times) at 7 hr. Scale bars=200 μm (significant difference between groups, # p<0.05 in comparison with control (o/c) and *p<0.05 for the comparison between fiber scaffolds, n=5).

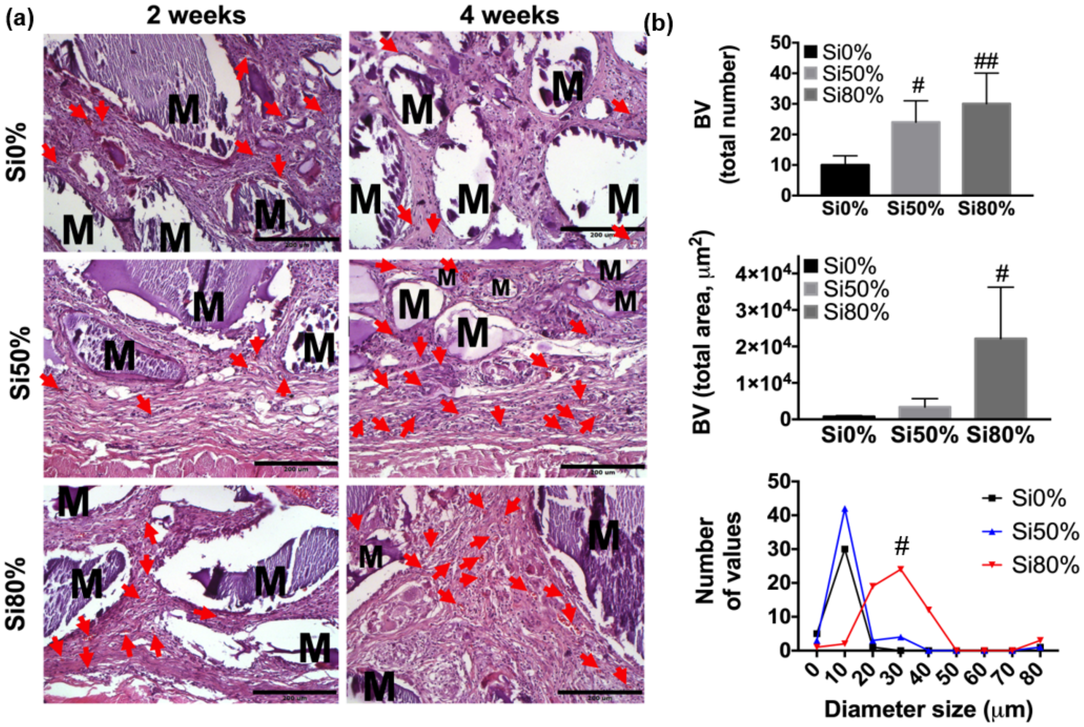

Figure 5. In vivo neo-blood vessel formation after fiber scaffold implantation in rat subcutaneous tissue. (a) Histological sections were analyzed by hematoxylin and eosin staining at 2 and 4 weeks. Red arrows mark the neo-formed blood vessels in each group, (b) quantified at 4 wks for comparison between the groups. In vivo implantation in subcutaneous tissue leading to more pronounced blood vessel formation around the silicate-shelled scaffold (especially Si80%) compared with the silicate-free scaffold. Scale bars= 200 μm (significant difference between groups, # $p<0.05$ and ## $p<0.01$, comparison with control (Si0%), n=4).

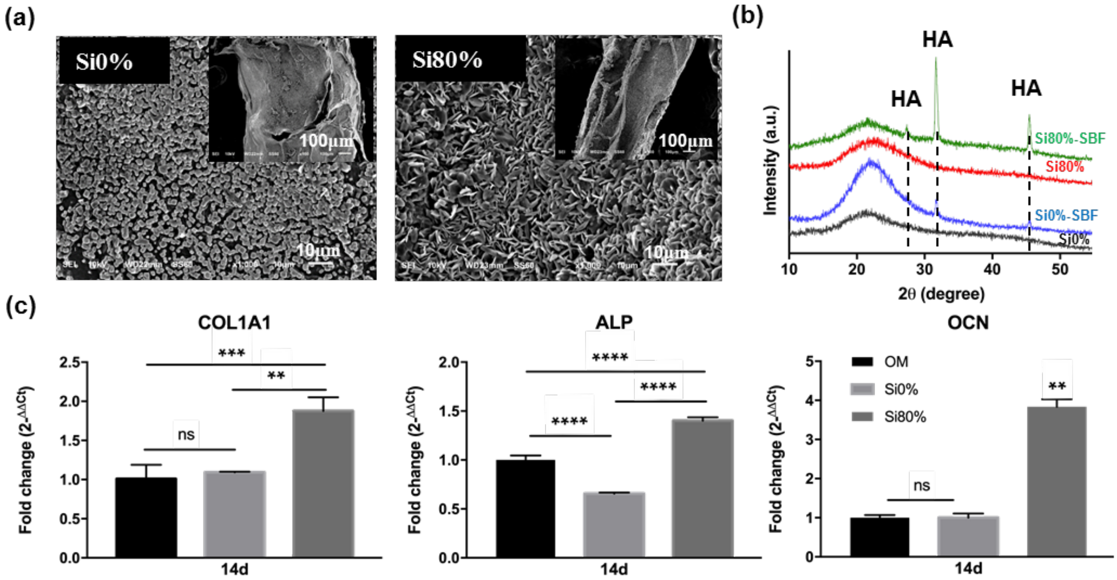

Figure 6. Osteogenic capacity from acellular hydroxyapatite (HA) formation and cellular osteogenic gene expression. Acellular HA formation was observed 14 days after fibers were immersed in SBF and were characterized by (a) SEM, revealing typical hydroxyapatite (HA)-like crystal morphology on the surface of Si80% scaffolds, and by (b) XRD spectra, confirming deposited crystals as HA. (c) The cellular osteogenesis potential of the silicate/alginate scaffolds was further proven by the enhanced expression of osteogenic genes (Col1a1, ALP and OCN) with rMSCs. (Significant difference between groups, ns (no significant difference), **p<0.01, ***p<0.001, ***<0.0001, n=3).

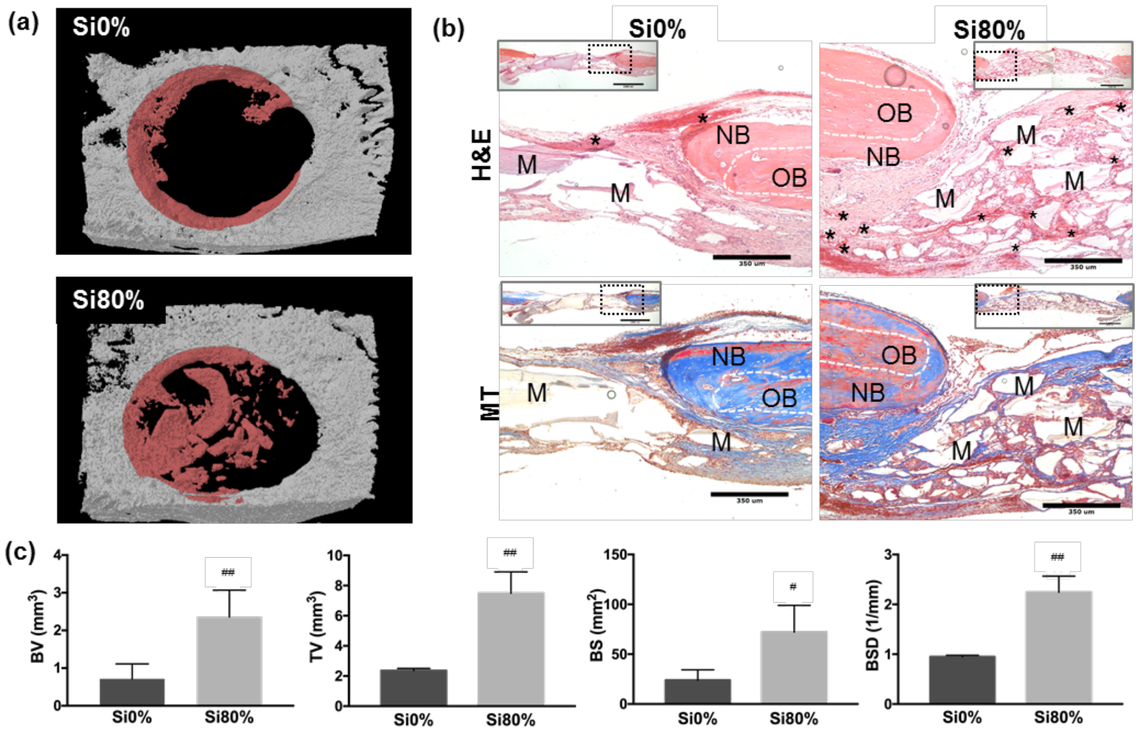

Figure 7. In vivo osteogenic capacity using a rat calvaria defect model. (a) After 6 weeks of implantation, μ-CT images were taken to reveal new bone, highlighted in red-brown. (b) H&E (hematoxylin & eosin) and MT (Masson's trichrome) staining at low and high magnification. New bone (NB), old bone (OB), border of OB and NB (green dotted line), material (M), blood vessel (*). (c) μ-CT quantitative analyses of bone volume (BV), surface (BS), surface density (BSD) and tissue volume (TV, the significant difference between groups, #<0.05, ##p<0.01, n=5). When implanted in a rat calvarium defect, the silicate-shelled scaffold demonstrated significantly improved bone formation (2-3 times higher in bone volume, surface area and density) with concurrent signs of proangiogenesis surrounding the implanted area.